Supporting Information

Seed-assisted growth of α-Fe_2O_3 nanorod arrays on reduced graphene oxide: A superior anode for high-performance Li-ion and Na-ion batteries

Dezhi Kong,[a,b] Chuanwei Cheng,[a,*] Ye Wang,[b] Bo Liu,[b] Zhixiang Huang,[b] and Hui Ying Yang [b,*]

[a]*Shanghai Key Laboratory of Special Artificial Microstructure Materials and Technology, School of Physics Science and Engineering, Tongji University, Shanghai 200092, P.R. China*
[b]*Pillar of Engineering Product Development, Singapore University of Technology and Design, 8 Somapah Road, Singapore 487372, Singapore*

Supporting Figures

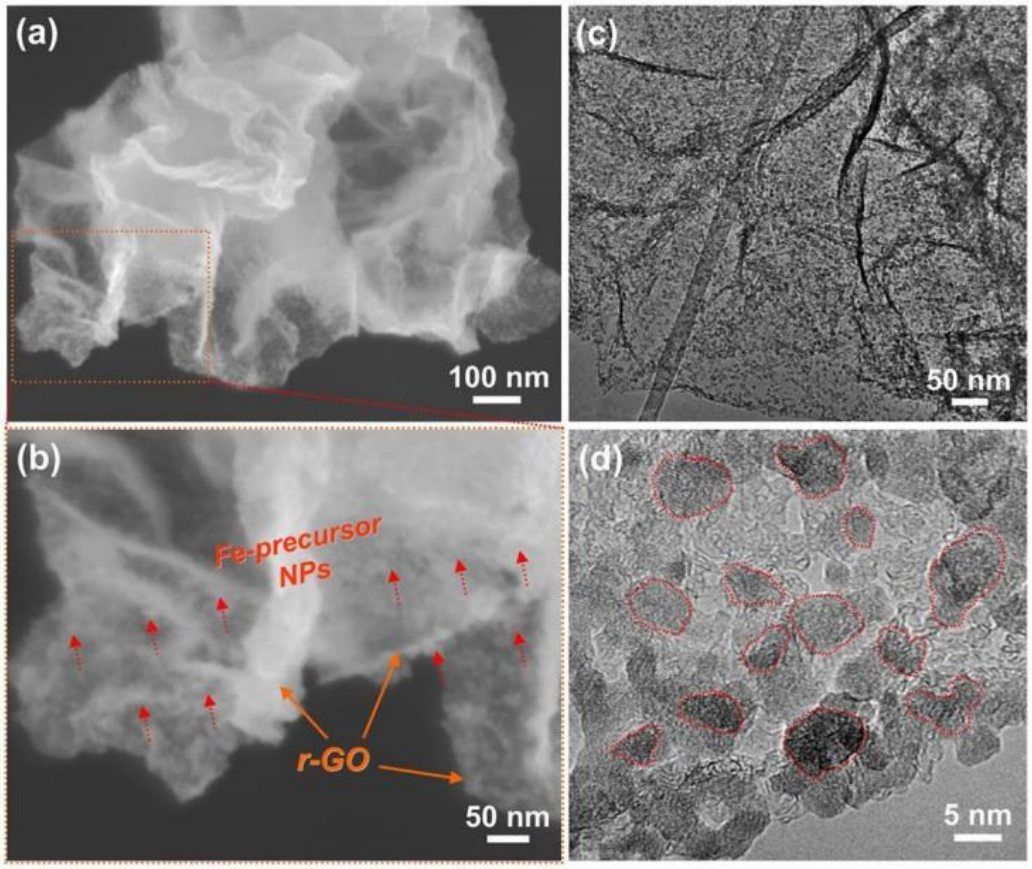

Fig. S1 Low-magnification (a) and enlarged (b) SEM images of r-GO were coated with Fe-precursor nanoparticles (Fe-precursor@r-GO NPs); Low-magnification (c) and enlarged (d) TEM images of r-GO were coated with Fe-precursor.

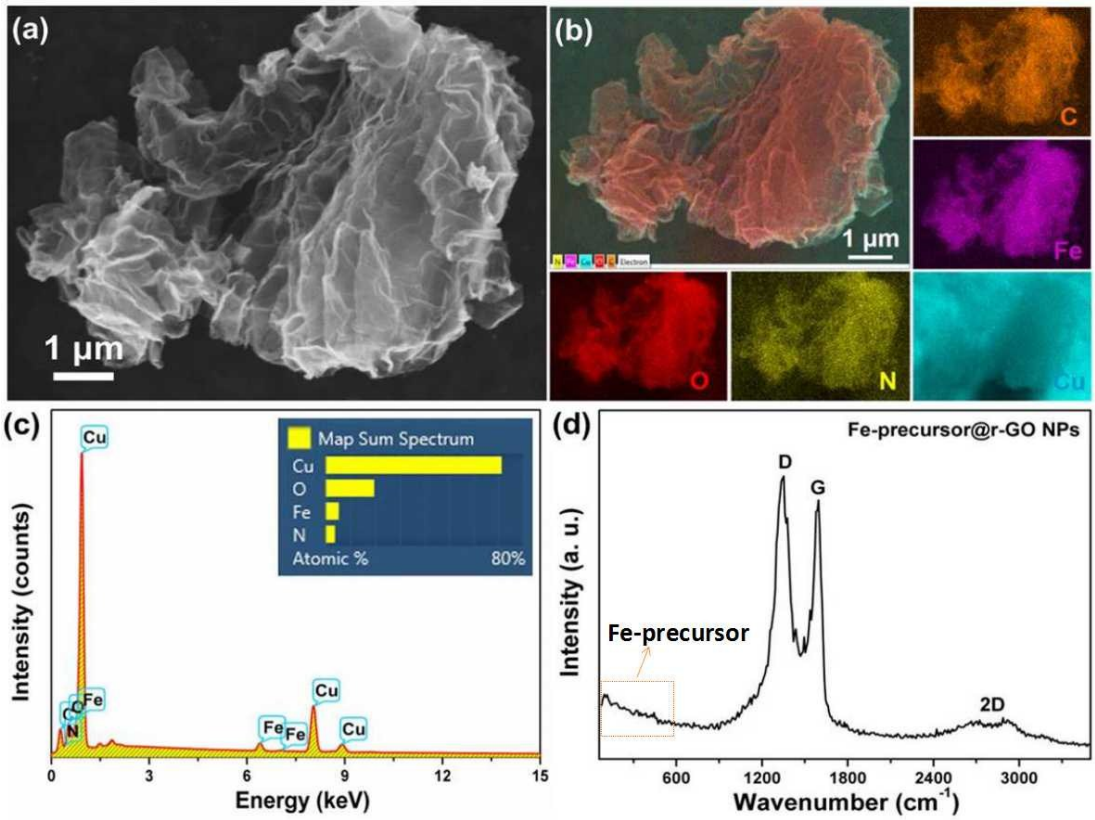

Fig. S2 (a) SEM image of r-GO were coated with Fe-precursor nanoparticles; (b) Corresponding EDS elemental mappings of C, Fe, O, N, and Cu for the Fe-precursor@r-GO NPs; (c) The EDS microanalysis and the corresponding elemental contents on selected areas of the Fe-precursor@r-GO NPs; (d) Raman spectra of Fe-precursor@r-GO NPs.

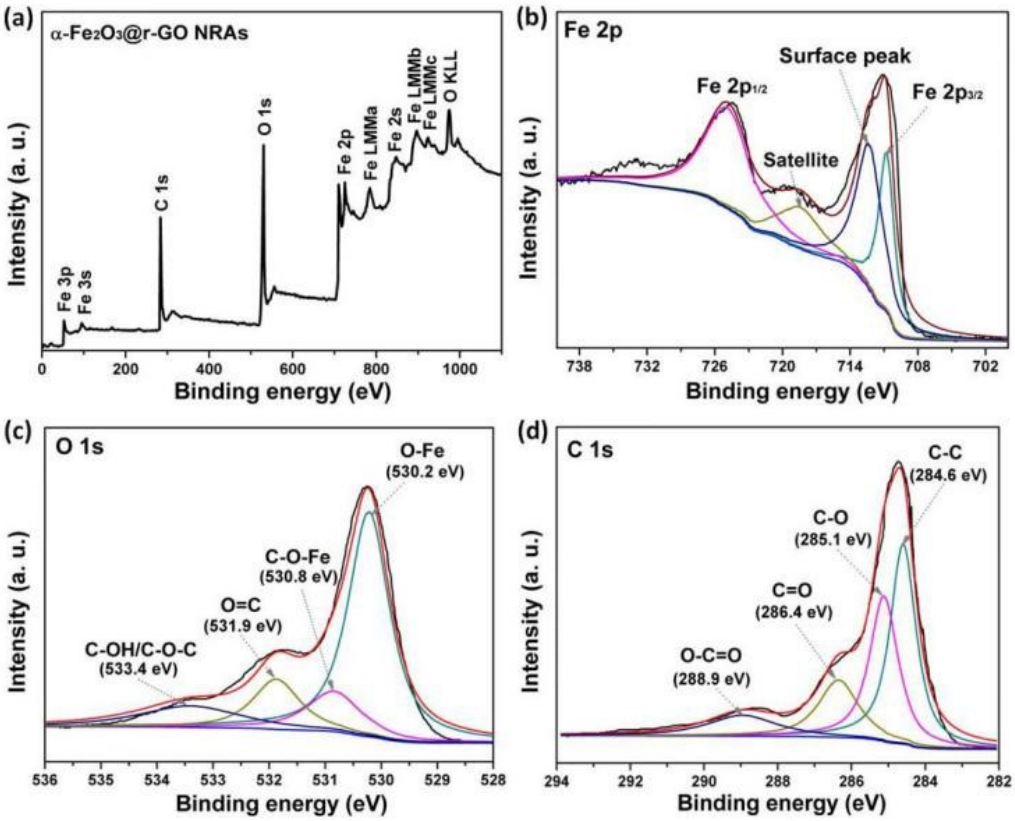

Fig. S3 XPS spectra: (a) wide scan, (b) high-resolution Fe 2p spectra, (c) high-resolution O 1s spectra, and (d) C 1s spectra of the α-Fe_2O_3@r-GO NRAs composite.

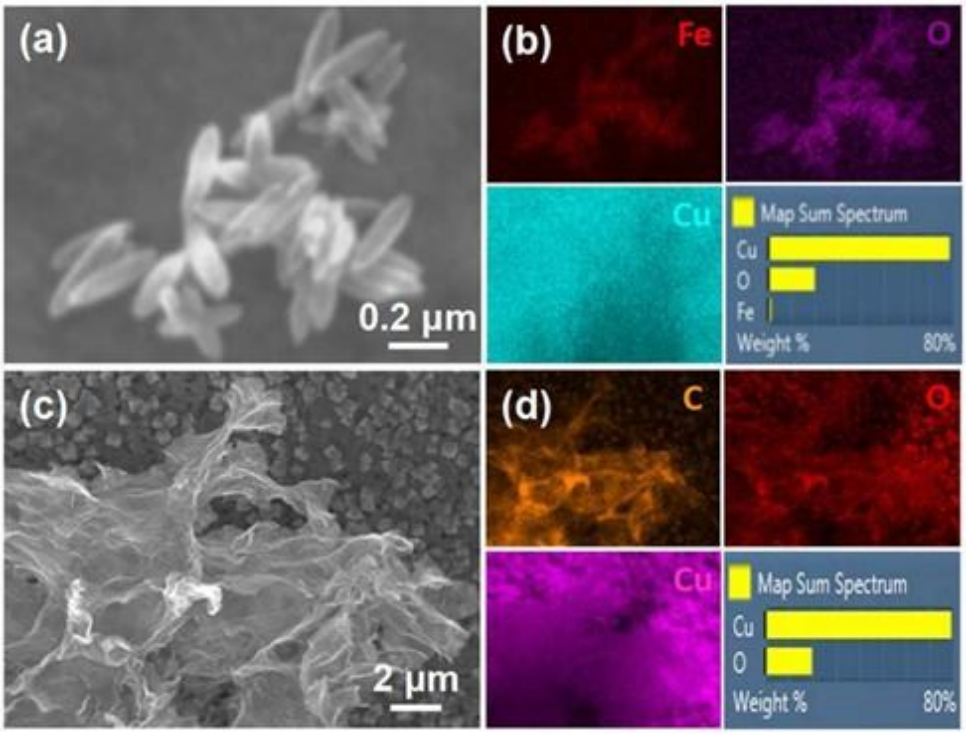

Fig. S4 (a, b) SEM image and corresponding EDS elemental mappings of Fe, O and Cu for the α-Fe_2O_3 NRs; (c, d) SEM image and corresponding EDS elemental mappings of C, O and Cu for the r-GO nanosheets.

The Morphology Evolution: Before the hydrothermal reaction, only some irregular Fe-precursor NPs are uniformly scattered on the surface of r-GO sheets (as shown in Fig. 6a). When a small amount of $FeCl_3$ (0.4 mmol) is added in this system, most Fe-precursor NPs have evolved into densely Fe-precursor nanosheet arrays (NSAs) standing upright on the surface of r-GO nanosheets (Fig. 6b). This suggests that heterogeneous nucleation of Fe-precursor nansheets on the r-GO sheets has been facilitated by the rapid hydrolysis process for lower Fe^{3+} concentrations. While the amount of $FeCl_3$ increase from 0.8 to 1.2 mmol, nanosheets-nanorods hybrid structures are obtained (Fig. 6c and d), which are evident that the rod-like α-Fe_2O_3 nanostructures begin to appear and the number of the nanorods gradually increase. This morphology change might be due to that the heterogeneous nucleation is impacted by the concentrations of Fe^{3+}. Increasing the amount of $FeCl_3$ to 1.6 mmol (Fig. 6e) results in the optimal morphology of α-Fe_2O_3 nanorod arrays, which densely standing and homogeneously distributed both on the surface of r-GO sheets. Upon further increasing the amount of $FeCl_3$ to 2.0 mmol (Fig. 6f), α-Fe_2O_3 mainly tended to grow into the 3D morphology (rods/flower-like) nanostructures, which consist of nanorods with the length ranging from dozens to hundreds of nanometers.

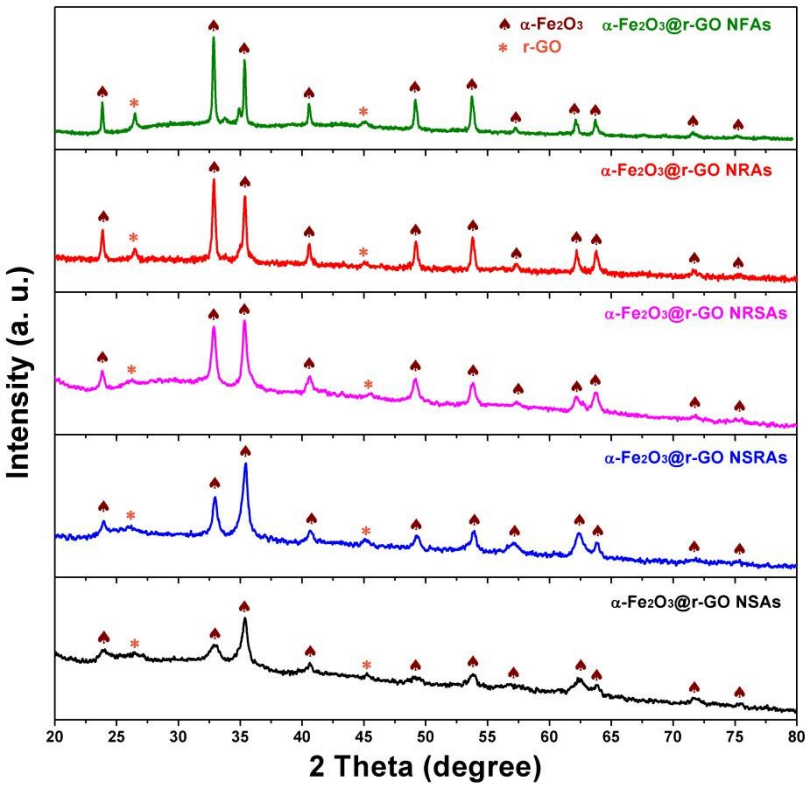

Fig. S5 XRD patterns of the *α*-Fe_2O_3@r-GO nanostructure arrays at different amounts of $FeCl_3$ during the second hydrothermal process: 0.4 mmol, 0.8 mmol, 1.2 mmol, 1.6 mmol, and 2.0 mmol (marked as *α*-Fe_2O_3@r-GO NRAs, *α*-Fe_2O_3@r-GO NSRAs, *α*-Fe_2O_3@r-GO NRSAs, *α*-Fe_2O_3@r-GO NRAs, and *α*-Fe_2O_3@r-GO NFAs, respectively).

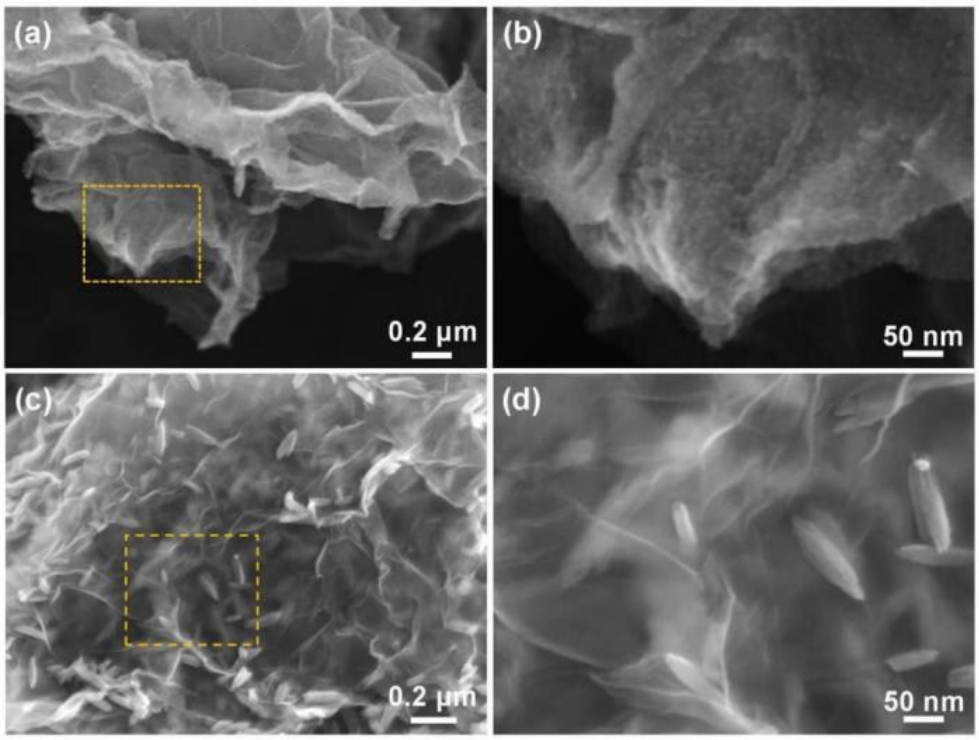

Fig. S6 (a, b) SEM images of the products obtained as the $NaNO_3$ were not added to the reaction system; (c, d) SEM images of the products obtained as the r-GO sheets without Fe-precursor seeds were added to the reaction system.

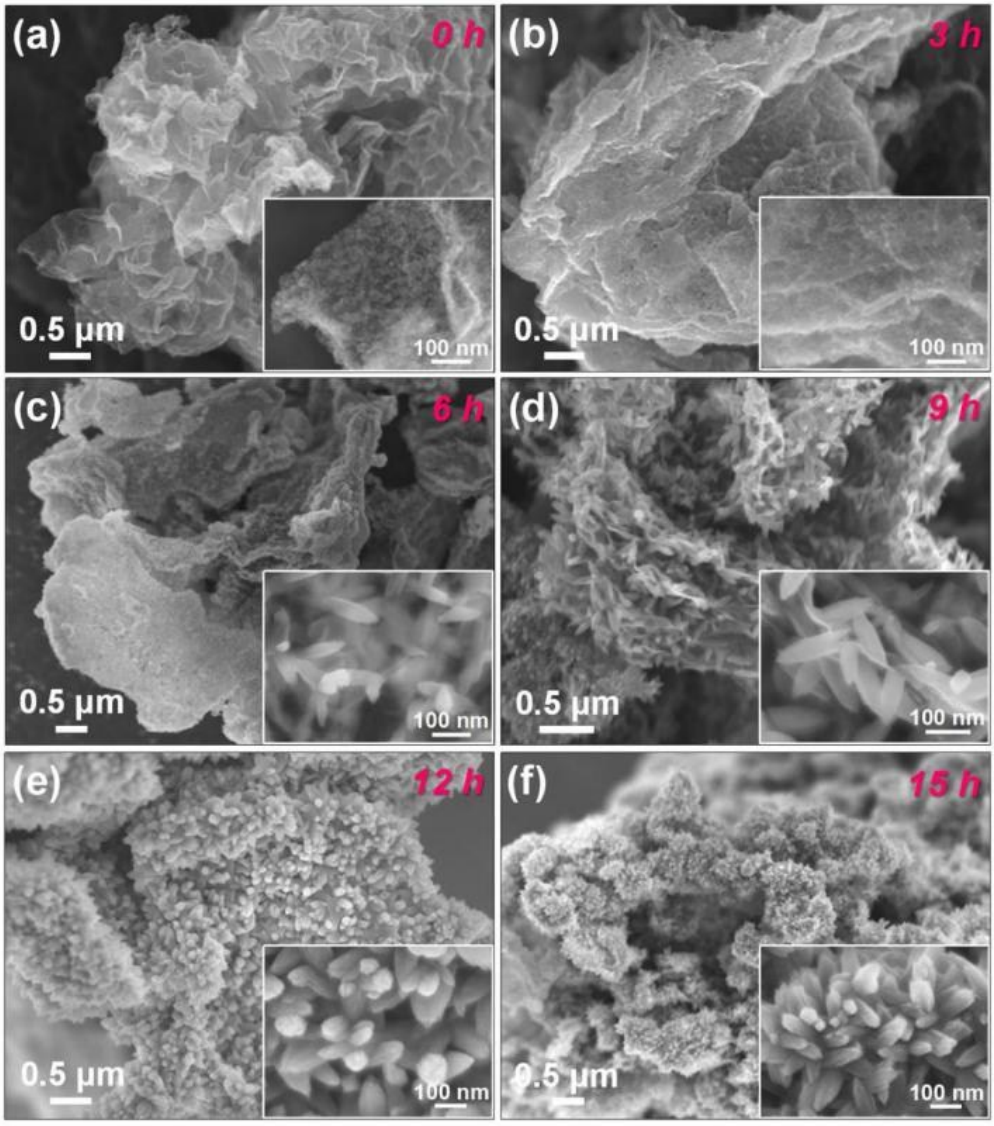

Fig. S7 Morphologies of the α-Fe_2O_3@r-GO NRAs during the second hydrothermal process at various reaction stages by setting the reaction time to (a) 0 h, (b) 3 h, (c) 6 h; (d) 9 h; (e) 12 h and (f) 15 h. In the beginning, the irregular Fe-precursor NPs are distributed onto r-GO nanosheets surface (Fig. S7a). When the hydrothermal reaction was extended to 2 h, some nanoparticles and nanorods are uniformly formed on the r-GO surface (Fig. S7b). As shown in Fig. S7c, after reaction for 6 h, some short α-Fe_2O_3 nanorods start grew on the surface of r-GO nanosheets. While to 9 h, the α-Fe_2O_3 nanorods became longer and partially covered on r-GO nanosheets surface (Fig. S7d). With the reaction time increased to 12 h, we can see that the well-ordered α-Fe_2O_3 NRAs formed and fully covered on r-GO sheets surface as shown by the SEM images in Fig. S7e. Nevertheless, upon increasing the reaction time to 15 h, the packing of nanorods becomes dense and some agglomeration starts to appear onto r-GO nanosheets surface (Fig. S7f).

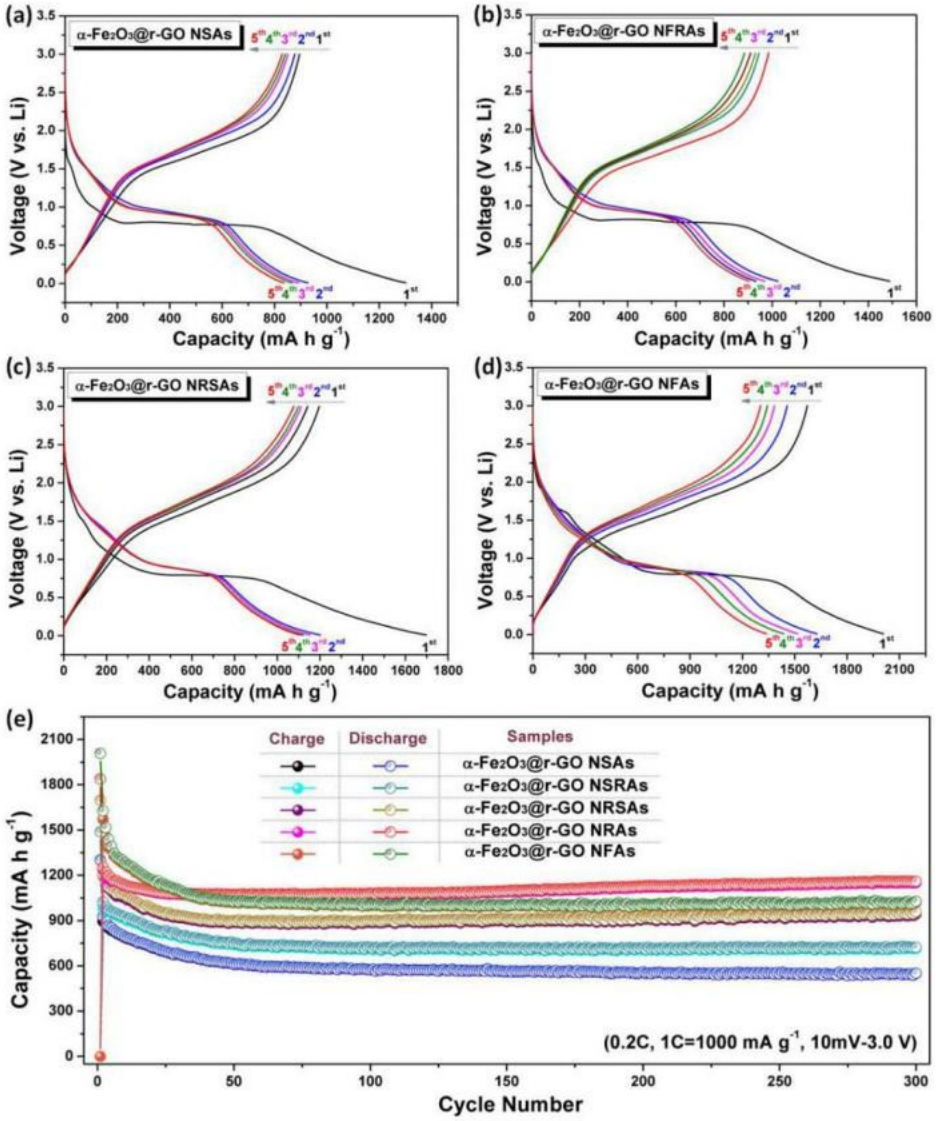

Fig. S8 Galvanostatic discharge/charge profiles of the α-Fe_2O_3@r-GO NSAs anode (a), α-Fe_2O_3@r-GO NSRAs anode (b), α-Fe_2O_3@r-GO NRSAs anode (c), and α-Fe_2O_3@r-GO NFAs anode (d) at a constant current density of 200 mA g^{-1}. (d) Cycling performance of the anodes at a constant current density of 200 mA g^{-1}.

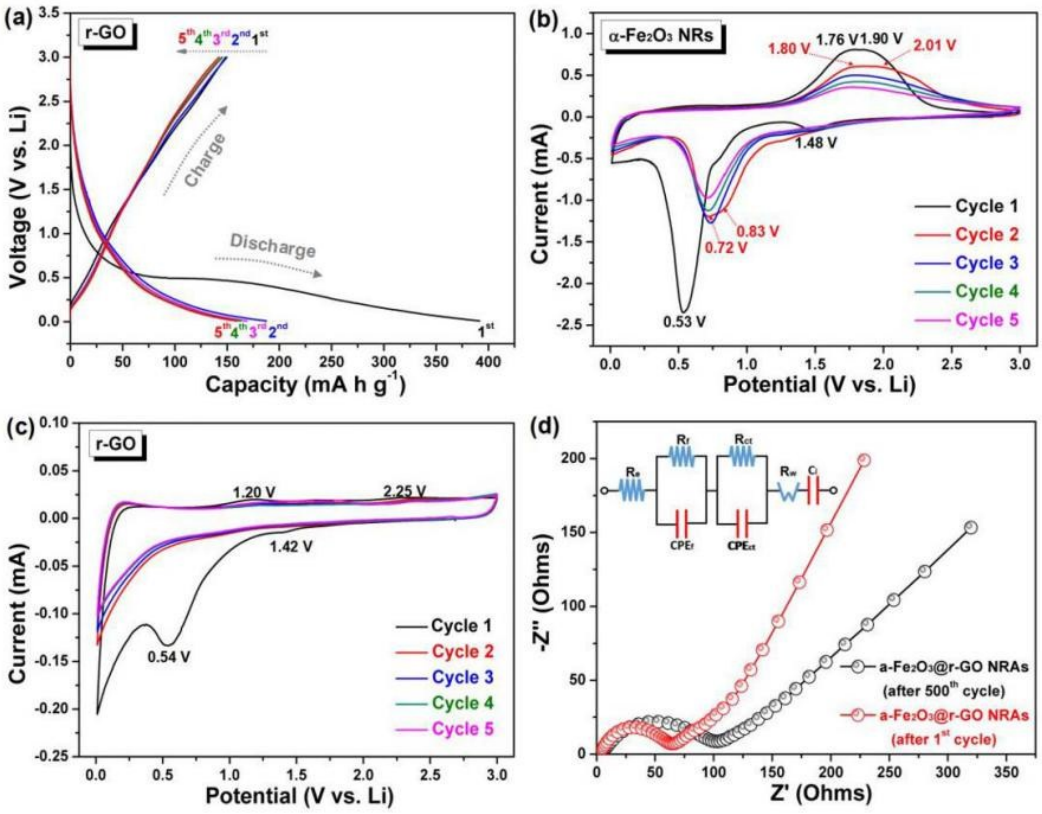

Fig. S9 (a) Galvanostatic discharge/charge profiles of original r-GO anode at a constant current density of 200 mA g^{-1}. CV curves of the pure α-Fe_2O_3 NRs anode (b) and the original r-GO anode (c) at 0.1 mV s^{-1} scanning rate. (d) Equivalent circuit and electrochemical impedance spectra of the α-Fe_2O_3@r-GO NRAs after the first and 500th cycles.

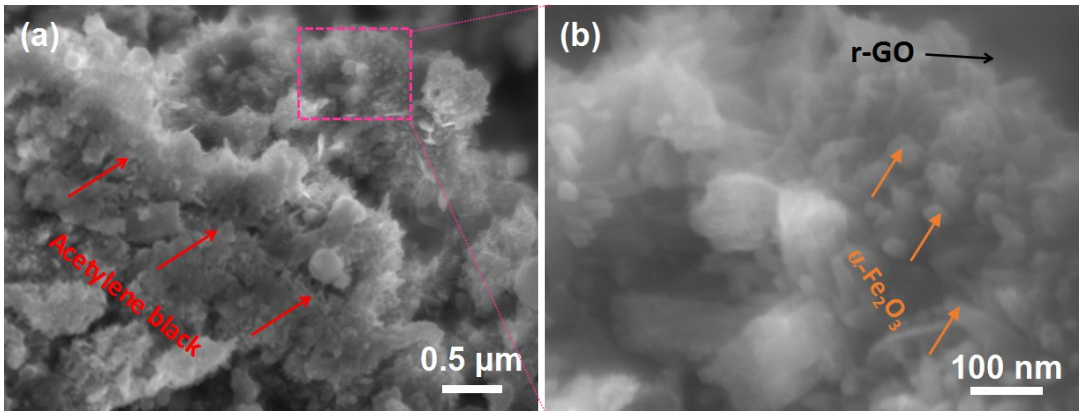

Fig. S10 (a) Low-magnification and (b) high-resolution SEM images of α-Fe_2O3 nanorods/r-GO composite after 500 cycling test.

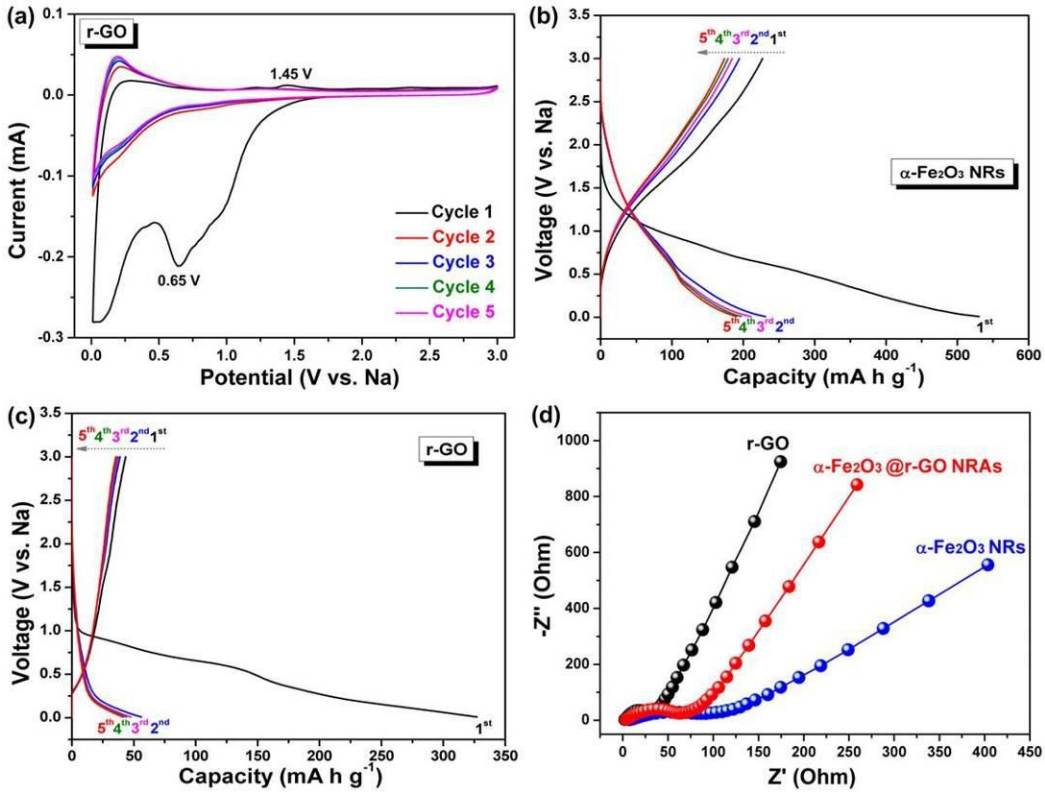

Fig. S11 (a) CV curves of the original r-GO anode at 0.1 mV s^{-1} scanning rate. Galvanostatic discharge/charge profiles of the pure α-Fe_2O_3 NRs anode (b) and the original r-GO anode (c) at a constant current density of 200 mA g^{-1}. (d) Equivalent circuit and electrochemical impedance spectra after the 1st cycle.

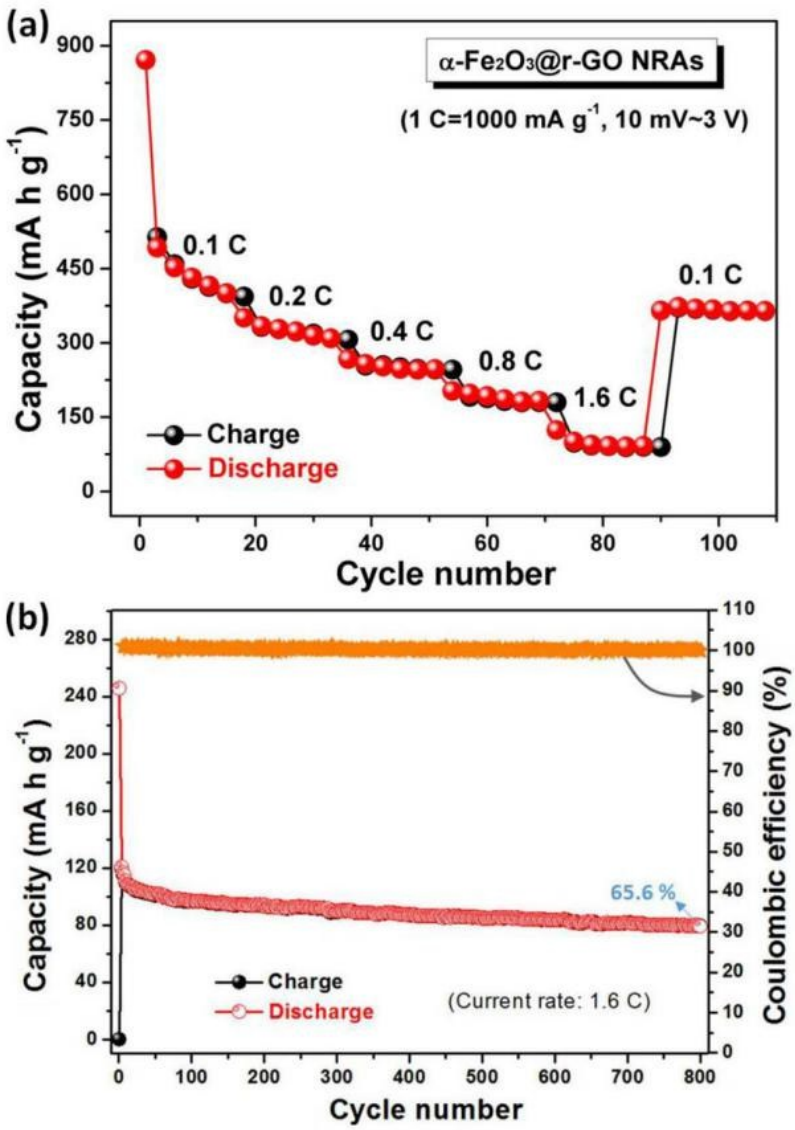

Fig. S12 (a) Reversible capacity vs. current density (rate capability) for the α-Fe_2O_3@r-GO NRAs anode. (b) Cycling performance of the α-Fe_2O_3@r-GO NRAs anode at a higher constant current density of 1.6 C.

Supporting Tables

Table S1 A survey of electrochemical properties of Fe_2O_3 (or r-GO)-based and theirs hybrid composites in lithium ion batteries.

Electrode description	Specific capacity (vs. Li, mA h g^{-1})	High rate capability (mA h g^{-1})	Cycling stability (%)	Ref.
α-Fe_2O_3@r-GO NRAs composite	1212 mAh/g at 200 mA/g between 0.01~3.0 V	776 mAh/g at 1600 mA/g	96.7 % after 500 cycles at 200 mA/g	**This work**
RG-O/Fe_2O_3 composite	1130 mAh/g at 200 mA/g between 0.005~3.0 V	~800 mAh/g at 800 mA/g	~82.2 % after 50 cycles at 100 mA/g	**[1]**
Fe_2O_3/GS Aerogels	1300 mAh/g at 100 mA/g between 0~3.0 V	370 mAh/g at 6000 mA/g	86.6 % after 500 cycles at 500 mA/g	**[2]**
40 wt.%-rGO/Fe_2O_3 composite	804 mAh/g at 45 mA/g between 0.01~3.0 V	280 mAh/g at 10000 mA/g	~83.3 % after 50 cycles at 45 mA/g	**[3]**
Fe_2O_3-graphene sheet-on-sheet composites	800.6 mAh/g at 100 mA/g between 0.005~3.0 V	792.2 mAh/g at 5000 mA/g	57.1 % after 100 cycles at 200 mA/g	**[4]**
Fe_2O_3/Fe_3C-graphene thin film	1118 mAh/g at 50 μA cm^{-2} between 0.01~3.0 V	~503 mAh/g at 1000 μA cm^{-2}	90 % after 1000 cycles at 1000 μA cm^{-2}	**[5]**
Fe_2O_3 rhombo-hedra/graphene composite	1025.2 mAh/g at 100 mA/g between 0.005~3.0 V	426.7 mAh/g at 1000 mA/g	85.7 % after 50 cycles at 100 mA/g	**[6]**
Fe_2O_3/G(H) (or Fe_2O_3/G(P)) composite	1130 mAh/g (or 320 mAh/g) at 200 mA/g between 0.005~3.0 V	634 mAh/g (for Fe_2O_3/G(H)) at 2000 mA/g	~99 % after 450 (or ~30% after 50) cycles at 200 mA/g	**[7]**
α-Fe_2O_3/r-GO composite	990 mAh/g at 100 mA/g between 0.005~3.0 V	-------	89.7 % after 50 cycles at 100 mA/g	**[8]**
nanorod-like Fe_2O_3/ graphene composite	1063.2 mAh/g at 100 mA/g between 0.005~3.0 V	210.7 mAh/g at 1000 mA/g	~50.6 % after 30 cycles at 100 mA/g	**[9]**
Fe_2O_3/r-GO nanocomposite	~1280 mAh/g at 50 mA/g between 0.005~3.0 V	~500 mAh/g at 600 mA/g	~81.5 % after 50 cycles at 50 mA/g	**[10]**
Fe_2O_3@C@G composite	~750 mAh/g at 100 mA/g between 0.01~3.0 V	430 mAh/g at 2000 mA/g	120 % after 100 cycles at 100 mA/g	**[11]**
Fe_2O_3/N-GS composite	1012 mAh/g at 100 mA/g between 0~3.0 V	-------	97 % after 100 cycles at 100 mA/g	**[12]**
Fe_2O_3-FLG composite	758 mAh/g at 200 mA/g between 0.01~3.0 V	295 mAh/g at 5000 mA/g	~89.1 % after 300 cycles at 200 mA/g	**[13]**
Fe_2O_3/rGO composite	600 mAh/g at 100 mA/g between 0.01~3.0 V	180 mAh/g at 10000 mA/g	~99.6 % after 300 cycles at 10000 mA/g	**[14]**
γ-Fe_2O_3 IVS-NRs/rGO nanocomposite	1284 mAh/g at 100 mA/g between 0.01~3.0 V	734 mAh/g at 5000 mA/g	73.2 % after 50 cycles at 100 mA/g	**[15]**
RGO-Fe_2O_3 nanocomposite	969 mAh/g at 100 mA/g between 0.01~3.0 V	336 mAh/g at 5000 mA/g	65.6 % after 100 cycles at 500 mA/g	**[16]**
HP-Fe-G composite	1200 mAh/g at 200 mA/g between 0.05~3.0 V	531 mAh/g at 5000 mA/g	77.7 % after 50 cycles at 200 mA/g	**[17]**
α-Fe_2O_3/RGO composite	1088 mAh/g at 200 mA/g between 0.005~3.0 V	512 mAh/g at 5000 mA/g	~75.8 % after 150 cycles at 1000 mA/g	**[18]**

Fe_2O_3-NC/GN aerogels	1140 mAh/g at 200 mA/g between 0.01~3.0 V	420 mAh/g at 6000 mA/g	108.5 % after 500 cycles at 500 mA/g	**[19]**
α-Fe_2O_3 nanorods	908 mAh/g at 201 mA/g between 0.01~3.0 V	837 mAh/g at 503 mA/g	121.3 % after 100 cycles at 503 mA/g	**[20]**
α-Fe_2O_3/graphene nanocomposite	588 mAh/g at 50 mA/g between 0.01~2.5 V	361 mAh/g at 3000 mA/g	93 % after 30 cycles at 1000 mA/g	**[21]**
rGO/α-Fe_2O_3 nano-plate composite	1149 mAh/g at 100 mA/g between 0.01~3.0 V	~475 mAh/g at 15000 mA/g	~99 % after 1000 cycles at 10000 mA/g	**[22]**
3D Fe_2O_3/RGO hydrogel	850 mAh/g at 200 mA/g between 0.01~3.0 V	280 mAh/g at 1000 mA/g	~69.4 % after 70 cycles at 200 mA/g	**[23]**
Fe_2O_3-GNS rice (or particle)-on-sheet composite	1184 mAh/g (or 1120 mAh/g) at 100 mA/g between 0.005~3.0 V	825 mAh/g (or ~780 mAh/g) at 1000 mA/g and 633 mAh/g (or ~600 mAh/g) at 5000 mA/g	~62 % (or ~27.9) after 40 cycles at 100 mA/g	**[24]**
α-Fe_2O_3/CNT-GF composite	900 mAh/g at 200 mA/g between 0.01~3.0 V	450 mAh/g at 3000 mA/g	~100 % after 300 cycles at 200 mA/g	**[25]**
nanohollow γ-Fe_2O_3 @graphene hybrid	1095 mAh/g at 100 mA/g between 0.01~3.0 V	504 mAh/g at 10000 mA/g	~76.1 % after 100 cycles at 1000 mA/g	**[26]**
porous α-Fe_2O_3 nanosheets on Ti foil	1140 mAh/g at 100 mA/g between 0.005~3.0 V	573 mAh/g at 2000 mA/g	~90 % after 60 cycles at 1000 mA/g	**[27]**
α-Fe_2O_3 nanorod arrays on Ti foil	950 mAh/g at 1000 mA/g between 0.05~3.0 V	350 mAh/g at 30000 mA/g	~102.4 % after 60 cycles at 1000 mA/g	**[28]**

Table S2 A survey of electrochemical properties of Fe_2O_3 (or r-GO)-based and theirs hybrid composites in sodium ion batteries.

Electrode description	Specific capacity (vs. Na, mA h g^{-1})	High rate capability (mA h g^{-1})	Cycling stability (%)	Ref.
α-Fe_2O_3@r-GO NRAs composite	~450 mAh/g at 100 mA/g between 0.01~3.0 V	~92 mAh/g at 1600 mA/g	~82.4 % after 300 cycles at 200 mA/g	**This work**
α-Fe_2O_3/rGO nanocomposite	~310 mAh/g at 100 mA/g between 0.05~3.0 V	~77 mAh/g at 2000 mA/g	~25.8 % after 150 cycles at 100 mA/g	**[29]**
Fe_2O_3-RGO (FG-30) composite	251.9 mAh/g at 100 mA/g between 0.005~3.0 V	32.8 mAh/g at 2000 mA/g	~68.8 % after 50 cycles at 50 mA/g	**[30]**
Fe_2O_3@GNS composite	~400 mAh/g at 100 mA/g between 0.005~3.0 V	110 mAh/g at 2000 mA/g	~75 % after 200 cycles at 200 mA/g	**[31]**
nanopore-structured γ-Fe_2O_3 film	450 mAh/g at 250 mA/g between 0.05~2.5 V	200 mAh/g at 1500 mA/g	90 % after 100 cycles at 250 mA/g	**[32]**
nanopore-structured γ-Fe_2O_3 film	345.7 mAh/g at 50 mA/g between 0.01~2.5 V	210.4 mAh/g at 200 mA/g	~36 % after 200 cycles at 250 mA/g	**[33]**
3D porous γ-Fe_2O_3 @C nanocomposite	~722.3 mAh/g at 200 mA/g between 0.04~3.0 V	317 mAh/g at 8000 mA/g	~74.5 % after 200 cycles at 200 mA/g	**[34]**
porous Fe_2O_3 films	386 mAh/g at 100 mA/g between 0.005~3.0 V	233 mAh/g at 5000 mA/g	~67 % after 100 cycles at 100 mA/g	**[35]**
nanostructured Fe_2O_3	350 mAh/g at 40 mA/g between 0.005~2.8 V	233 mAh/g at 130 mA/g	~71.4 % after 60 cycles at 130 mA/g	**[36]**
SnO_2@graphene nanocomposite	569 mAh/g at 40 mA/g between 0.01~3.0 V	143 mAh/g at 640 mA/g	~91 % after 100 cycles at 20 mA/g	**[37]**
3D WS_2-RGO microsphere	404 mAh/g at 100 mA/g between 0.01~3.0 V	287 mAh/g at 900 mA/g	~93 % after 200 cycles at 200 mA/g	**[38]**
MoS_2/graphene composite paper	240 mAh/g at 25 mA/g between 0.01~2.25 V	173 mAh/g at 200 mA/g	~83 % after 20 cycles at 25 mA/g	**[39]**
SnS_2-RGO composite	~670 mAh/g at 100 mA/g between 0.01~2.5 V	~544 mAh/g at 2000 mA/g	84 % after 500 cycles at 1000 mA/g	**[40]**

References

[1] X. J. Zhu, Y. W. Zhu, S. Murail, M. D. Stoller and R. S. Ruoff, *ACS Nano*, 2011, **5**, 3333-3338.

[2] R. H. Wang, C. H. Xu, M Du, J. Sun, L. Gao, P. Zhang, H. L. Yao and C. C. Lin, *Small*, 2014, **10**, 2260-2269.

[3] I. T. Kim, A. Magasinski, K. Jacob, G. Yushin and R. Tannenbaum, *Carbon*, 2013, **52**, 56-64.

[4] J. Kan and Y. Wang, *Sci. Rep.*, 2013, **3**, 3502.

[5] Y. Yang, X. J. Fan, G. Casillas, Z. W. Peng, G. D. Ruan, G. Wang, M. J. Yacaman and J. M. Tour, *ACS Nano*, 2014, **8**, 3939-3946.

[6] Y. Jiang, X. T. Ling, X. H. Cai, Z. Jiao and L. L. Cheng, *J. Mater. Res.*, 2015, **30**, 761-769.

[7] H. W. Zhang, L. Zhou and C. Z. Yu, *RSC Adv.*, 2014, **4**, 495-499.

[8] D. Z. Chen, W. Wei, R. N. Wang, J. C. Zhu and L. Guo, *New J. Chem.*, 2012, **36**, 1589-1595.

[9] B. Zhao, R. Z. Liu, X. H. Cai, Z. Jiao, M. H. Wu, X. T. Ling, B. Lu and Y. Jiang, *J Appl Electrochem*, 2014, **44**, 53-60.

[10] S. Y. Liu, J. Xie, Q. Pan, C. Y. Wu, G. S. Cao, T. J. Zhu and X. B. Zhao, *Int. J. Electrochem. Sci.,* 2012, **7**, 354-362.

[11] H. L. Fei, Z. W. Peng, L. Li, Y. Yang, W. Lu, E. L. G. Samuel, X. J. Fan and J. M. Tour, *Nano Res.*, 2014, **7**, 502-510.

[12] M. Du, C. Xu, J. Sun and L. Gao, *Electrochim. Acta*, 2012, **80**, 302-307.

[13] Y. K. Wang, L. C. Yang, R. Z. Hu, W. Sun, J. W. Liu, L. Z. Ouyang, B. Yuan, H. H. Wang and M. Zhu, *J. Power Sources*, 2015, **288**, 314-319.

[14] L. S. Xiao, M. Schroeder, S. Kluge, A. Balducci, U. Hagemann, C. Schulz and H. Wiggers, *J. Mater. Chem. A*, 2015, **3**, 11566-11574.

[15] X. L. Wang, J. Mujtaba, F. Fang, M. Ahmad, H. Arandiyan, H. P. Yang, G. X. Sun and H. Y. Sun, *RSC Adv.*, 2015, **5**, 91574-91580.

[16] S. Bai, S. Q. Chen, X. P. Shen, G. X. Zhu and G. X. Wang, *RSC Adv.*, 2012, **2**, 10977-10984.

[17] X. Wang, W. Tian, D. Q. Liu, C. Y. Zhi, Y. Bando and D. Golberg, *Nano Energy*, 2013, **2**, 257-267.

[18] J. Qu, Y. X. Yin, Y. Q. Wang, Y. Yan, Y. G. Guo, W. G. Song, *ACS Appl. Mater. Interfaces*, 2013, **5**, 3932-3936.

[19] R. H. Wang, C. H. Xu, J. Sun and L. Gao, *Sci. Rep.,* 2014, **4**, 7171.

[20] Y. M. Lin, P. R. Adam, A. Heller and C. B. Mullins, *J. Phys. Chem. Lett.*, 2011, **2**, 2885-2891.

[21] X. Y. Xue, C. H. Ma, C. X. Cui and L. L. Xing, *Solid State Sciences*, 2011, **13**, 1526-1530.

[22] S. K. Liu, Z. X. Chen, K. Xie, Y. J. Li, J. Xu and C. M. Zheng, *J. Mater. Chem. A*, 2014, **2**, 13942-13948.

[23] W. W. Zhou, C. Y. Ding, X. T. Jia, Y. Tian, Q. T. Guan and G. W. Wen, *Materials Research Bulletin*, 2015, **62**, 19-23.

[24] Y. Q. Zou, J. Kan and Y. Wang, *J. Phys. Chem. C*, 2011, **115**, 20747-20753.

[25] M. H. Chen, J. L. Liu, D. L. Chao, J. Wang, J. H. Yin, J. Y. Lin, H. J. Fan and Z. X. Shen, *Nano Energy*, 2014, **9**, 364-372.

[26] J. T. Hu, J. X. Zheng, L. L. Tian, Y. D. Duan, L. P. Lin, S. H. Cui, H. Peng, T. C. Liu, H. Guo, X. W. Wang and F. Pan, *Chem. Commun.,* 2015, **51**, 7855-7858.

[27] L. L. Li, H. B. Wu, L. Yu, S. Madhavi and X. W. Lou, *Adv. Mater. Interfaces*, 2014, **1**, 1400050.

[28] S. Chen, Y. L. Xin, Y. Y. Zhou, F. Zhang, Y. R. Ma, H. H. Zhou and L. M. Qi, *J. Mater. Chem. A*, 2014, **2**, 20022-20029.

[29] Z. J. Zhang, Y. X. Wang, S. L. Chou, H. J. Li, H. K. Liu and J. Z. Wang, *J. Power Sources*, 2015, **280**, 107-113.

[30] X. J. Liu, T. Q. Chen, H. P. Chu, L. Y. Niu, Z. Sun, L. K. Pan and C. Q. Sun, *Electrochim. Acta*, 2015, **166**, 12-16.

[31] Z. L. Jian, B. Zhao, P. Liu, F. J. Li, M. B. Zheng, M. W. Chen, Y. Shi and H. S. Zhou, *Chem. Commun.,* 2014, **50**, 1215-1217.

[32] B. Sun, S. J. Bao, J. L. Xie and C. M. Li, *RSC Adv.*, 2014, **4**, 36815-36820.

[33] S. B. Wang, W. Wang, P. Zhan and S. Q. Jiao, *ChemElectroChem*, 2014, **1**, 1636-1639.

[34] N. Zhang, X. P. Han, Y. C. Liu, X. F. Hu, Q. Zhao and J. Chen, *Adv. Energy Mater.*, 2015, **5**, 1401123.

[35] Y. Z. Jiang, M. J. Hu, D. Zhang, T. Z. Yuan, W. P. Sun, B. Xu and M. Yan, *Nano Energy*, 2014, **5**, 60-66.

[36] M. Valvo, F. Lindgren, U. Lafont, F. Björefors and K. Edström, *J. Power Sources*, 2014, **245**, 967-978.

[37] D. W. Su, H. J. Ahn and G. X. Wang, *Chem. Commun.,* 2013, **49**, 3131-3133.

[38] S. H. Choi and Y. C. Kang, *Nanoscale*, 2015, **7**, 3965-3970.

[39] L. David, R. Bhandavat and G. Singh, *ACS Nano*, 2014, **8**, 1759-1770.

[40] B. H. Qu, C. Z. Ma, G. Ji, C. H. Xu, J. Xu, Y. S. Meng, T. H. Wang and J. Y. Lee, *Adv. Mater.*, 2014, **26**, 3854-3859.